Doxorubicin and siRNA Co-Delivery System Based on Carbon Dots Inhibits Chemoresistance of Lung Cancer

Hui Luo
Sun Yat-sen University First Affiliated Hospital
Kexin Tang
Sun Yat-sen University First Affiliated Hospital
Kaichen Huang
Sun Yat-Sen University
Xi Lin
Sun Yat-sen University First Affiliated Hospital
Chaoming Mei
Sun Yat-sen University First Affiliated Hospital
Lili Wu
Harbin Normal University
Lei Yang
Harbin Institute of Technology
Hailing Yu (seal101010@163.com)
Sun Yat-Sen University https://orcid.org/0000-0001-8004-6444

Research

Keywords: chemoresistance, co-delivery, siRNA, carbon dots, MRP1

Posted Date: January 27th, 2021

DOI: https://doi.org/10.21203/rs.3.rs-123606/v2

Abstract

Background

The resistance to the anti-cancer agent limits the chemotherapy effect in the cancer therapy. Tumor easily develops resistance to anti-cancer drugs leading to decreased therapy efficiency of chemotherapies. Targeting signaling molecules related with chemoresistance through strategy of co-delivery siRNA and chemotherapeutics may overcome the multidrug resistance to chemotherapy. A co-delivery nanosystem that could carry siRNA and DOX simultaneously has been studied in this work.

Results

The co-delivery is based on carbon dots was surface-modified with poly-ethylenimine (PEI), and loaded the siMRP1 and chemotherapeutics by electronstatic interactions on the surface with pH-triggered drug release. The CD-PEI was synthesized by one-step microwave assisted method; the PEI were raw materials and passivator during the reaction process that makes CD exhibit excellent optical property and the capability of loading siRNA. The CD-PEI was capable of loading and delivering siMRP1 and DOX to tumor and release synchronously in cell by pH-triggered manner using flow cytometry and confocal laser scanning microscopy analysis. MRP1 was successfully knocked down by siRNA. The silencing of MRP1 by co-delivery system could increase DOX accumulation and significantly enhance the inhibitory effect of metastatic potential elicited by doxorubicin in A549 and A549/ADM cells.

Conclusion

The co-delivery systems effectively loaded and released siRNA and DOX agents to the targeted tumor, overcoming the resistant to chemotherapy. By suppressing MRP1, CD-PEI-DOX-siMRP1 can obviously increase the drug intercellular accumulation and inhibit the cell proliferation, migration and invasion, implying its potential application in enhancing therapeutic efficiency in clinical practices.

Background

Chemotherapy is the most useful therapy for cancer[1]. However, due to lack of effective targeted delivery, drug resistance always occurs during the chemotherapy process, and gives rise to the recurrence rate[2, 3]. Cancer cells possessing the multidrug resistance could inhibit the cellular internalization of the chemotherapeutics and reduce the therapeutic effect because of overexpression of ATP-binding cassettes which pump out of the drugs[4]. Effective delivery of drug to the targeted tissue could accumulate high drug concentration and weaken the side effects. With the advance of nanotechnology, nanomaterials have the potential to carry and selectively release the chemotherapeutics targeted to the cancer, leading to increased therapy efficacy. Co-delivery siRNA and chemotherapeutics may overcome the multidrug resistance to chemotherapy[5]. Polymer nanoparticles, liquid nanoparticles, and nonorganic nanoparticles have been used as a nanoplatform for co-delivery siRNA and drug[6]. However, the co-

delivery needs the synthesis of nanocarrier complex, and the selective release of co-loaded agents is fairly difficult.

Carbon dots (CD) is a novel kind of the quantum-sized nanomaterials, which have enormous application potential in bio-imaging, drug carrier, and nanosystems[7-9]. The application of semi-conductor quantum dots (QDs) is limited by the toxic of heavy metal. However, the carbon dots are composed by carbon atoms, which have excellent inherent biocompatibility, have the feasibility in the biotechnology application. CD have the capability of carry chemotherapeutic to the tumor and decrease cytotoxicity and enhance chemotherapy efficacy[10], and the CD with surface-modified groups can carry multiple drugs simultaneously[11, 12].

Lung cancer was reported to be easily resistant to drugs after several cycles of chemotherapy[13]. Doxorubicin was widely used in treating lung cancer. A plethora of proteins were identified in resistance against chemotherapy drugs in treating lung cancer. Multidrug resistant protein 1 (MRP1) is a pivotal member of ABCC subfamily belonging to ATP-binding cassette transporter superfamily, which transport anti-cancer drugs out of cells thus reducing the treatment efficacy[14]. How MRP1 was involved in chemoresistance against doxorubicin was elusive[15]. Whether MRP1 was involved in uptake of doxorubicin and influencing therapeutic efficacy of it warrants further study. Using small interfering RNA (siRNA) to downregulate proteins associated with multidrug resistance, such as MRP1, is a promising method for reversing drug resistance[16].

In this work, the CD are fabricated by microwave and passivized by polyethyleneimine (PEI). There are a lot of functional groups at the surface of CD due to the addition of PEI during the microwave synthesis process. The surface of CD is modified by PEI, as a passivation agent, in order to enhance the fluorescence intensity of CD and possess the capability of loading and delivery siRNA. The siRNA and DOX anti-cancer agents are delivery simultaneously to the targeted tumor by the CD with surface-modified PEI. By suppressing drug efflux pumps, the intercellular uptake is increased and more drugs located at the perinuclear regions. And the co-delivery system incorporating suppression of MRP1 and anticancer agents could enhance anti-cancer efficacy against chemoresistance in the lung cancer. The real-time tracking of the delivery process is realized through the excellent optical property of co-delivery carrier. Results from our study would deepen the regulator network of MRP1 in modulating chemoresistance of malignant cancer. It would fasten the clinical potential of co-delivery system with a combination of chemotherapeutics and siRNA sequences.

Results And Discussion

The characteristic of CD-PEI and nanodrug system based on CD-PEI

The TEM images showed that the CD-PEI was uniform and spherical, with an average size of 4.25 nm which obtained by measuring the sizes of hundreds CD nanoparticals in TEM images. It is indicated that the average diameter of CD-PEI is 5.503 nm measured by dynamic light scattering (DLS). CD-PEI was dark yellow under white light and well-distributed in aqueous solution. Under the UV light, the CD-PEI

solution had obvious green emission indicating that CD-PEI had excellent fluorescence property, as shown in Fig. S1. The photoluminescence (PL) spectra of CD-PEI and CD-PEI-DOX-siMRP1 had been characteristic by various excitation wavelengths with 20 nm increments. The emissions of CD are red-shifted with the increase of the excitation wavelength. The emission in CD could result from the surface effects and nanometer quantum confinement effect[17, 18]. The PL spectra of CD-PEI and CD-PEI-DOX-siMRP1 were obviously different. Due to the loading of DOX agents, the PL and UV-vis spectrum has changed. The emission intensity of CD-PEI-DOX-siMRP1 is lower than that of CD-PEI in spectra, and the peaks have red-shift. The increase of emission peak confirmed the DOX has been successfully loaded on the surface of CD-PEI[19]. The CD-PEI exhibited excellent and stable PL property that is beneficial for the tracking of drug delivery *in vivo*. In addition, the CD-PEI possess excitation-dependent emission behavior[20, 21], that when the excitation wavelength increase from 330 nm to 510 nm, the emission peak shift from 450 to 600 nm. When the excitation wavelength is 350 nm, the emission intensity is highest. In this work, we studied the PL behavior of CD-PEI-DOX-siMRP1 through increasing excitation wavelength from 270 to 510 nm. The CD-PEI-DOX-siMRP1 had no obvious emission peak when the excitation wavelength is lower than 330 nm. When excitation wavelengths increase from 350 nm to 510 nm, the emission intensity of CD-PEI-DOX-siMRP1 is increasing, and reaches maximum at 470 nm. The CD-PEI-DOX-siMRP1 has two emission peak centers at 560 and 690 nm.

There is obvious absorption band correspond to the O-H stretching in the FTIR spectrum of the CD. The absorption peaks centered at 1096 cm^{-1} and 1655 cm^{-1} are corresponded to the C-O and C=O stretching, respectively. The absorption bands at 1453 cm^{-1} and 2949 cm^{-1} are corresponded to the C-H and CH_2 stretching, respectively. The UV-Vis spectrum of CD-PEI had two bands at 304 nm and 346 nm, corresponding to the π-π^* transition and n-π^* transition[22-24]. The CD-PEI-DOX, CD-PEI-DOX-siNC, and CD-PEI-DOX-siMRP1 had a broad peak band at 480-600 nm among which was the DOX characteristic absorbance peak. These results confirmed that the DOX was loaded on the surface of CD-PEI, and the drug loading efficiency of CD-PEI was 16.7%.

The drug release behavior of CD-PEI-DOX-siMRP1 was revealed by *in vitro* release test. The free DOX release totally during 50 hours, while CD-PEI-DOX-siMRP1 prolong the drug release time up to 72 hours when pH was 5.2. CD-PEI-DOX-siMRP1 released fairly minimal DOX under pH 7.4 and illustrated that the nanocarrier would avoid the detrimental release of DOX in normal tissue and cell. When the pH changed from 7.4 to 5.2, the release amount of DOX from CD-PEI-DOX-siMRP1 increased about 5-times indicating that CD-PEI-DOX-siMRP1 was pH-sensitivity and triggered the release of DOX by acid environment because the water solubility of DOX was increased at lower pH. The advantage of selective drug release behavior of nanosystem could enhance the therapeutic effect of tumor and decrease the toxic to normal tissue.

The information of the chemical composition and functional groups of nanodrug were characterized by X-ray photoelectron spectroscopy (XPS) in Fig. 1I. As shown in Fig. 1, the XPS spectra of CD-PEI-DOX-siMRP1 exibit three peaks corresponding to C1s peak at 284.5 eV, N1s peak at 399.5 eV, and O1s peak at 531.5 eV, respectively. This result indicates that CD-PEI-DOX-siMRP1 are mainly composed of C, N, and O,

with some small inorganic elements due to the synthesis while attaining a solution system at pH 7.4 with PBS[25]. The C1s spectrum of CD-PEI-DOX-siMRP1 (Fig. 1J) shows four peaks at 284.8 eV, 285.8 eV, 287.7 eV, and 288.3 eV, which are attributed to C-C/C=C (78.4%), C-N/C-OH (16.4%), C=O (2.7%), and O-C=O (2.5%), respectively. The N1s spectrum of CD-PEI-DOX-siMRP1 (Fig. 1k) exhibits two components located at 398.9 eV and 400.2 eV, assigned to C=C-N (80.5%) and N-$(C)_3$ (19.5%) groups. The O1s spectrum of CD-PEI-DOX-siMRP1 (Fig. 1L) shows two peaks at 531.0 eV and 531.9 eV, which are corresponded to the C=O (47.7%) and C-OH/C-O-C (52.3%) groups. As shown in Table S1, the change in the chemical groups and the percentage of them in the spectra gives further evidence of successful complex conjugation.

MRP1 was involved in chemoresistance of A549 against CD-PEI-DOX.

Failure of the chemotherapy to malignant tumor was mainly attributable to insensitivity to drugs. Elucidating the mechanisms how tumor cells modulate the chemoresistance was critical for improving the chemotherapeutic effect of various drugs. We previously confirmed that CD-PEI-DOX treatment in hepatocellular carcinoma inhibit tumor growth through actively targeting tumors[10]. This led us to postulate: whether CD-PEI-DOX would elicit side effects on malignant tumors such as increasing chemoresistance in lung cancer. We firstly detected the expression of molecules associated with chemoresistance including p-glycoprotein (P-gp), MRP1, and ABCG2 in adherent, sphere and chemoresistant lung cancer cell line A549. From Fig. 3A, we vividly observed that molecules related with chemoresistance were elevated in spheres formed by A549 cells, which were considered to bear more traits of stemness compared with adherent cells. Consistently, the expression of these molecules elevated most in A549/ADM cells. These results show that A549/ADM cells expressed a panel of molecules involved in chemoresistance. Subsequently, we analyzed the cell viability of A549 and chemoresistant A549/ADM cells after doxorubicin treatment (Fig.3B). We discovered that A549/ADM cells were resistant to doxorubicin treatment. To investigate the involvement of MRP1 in chemoresistance of A549 against doxorubicin, we tentatively knockdown the expression of MRP1 using siRNA transfection. We determined the best knockdown efficiency of siRNA targeting MRP1 using qPCR methods. From Fig. 3C and 3D, we determined siRNA #2 was the most efficient sequence targeting MRP1. CD-PEI-DOX were conjugated with this sequence with best efficiency and CCK8 assays were performed to analyze the cell viability after treatment by various drugs. The IC_{50} of drugs in both A549 and A549/ADM cells were calculated from three independent cell toxicity experiments. As shown in Fig. 4A-4B and Table 1, free doxorubicin in A549/ADM cells was approximately 5 fold higher compared with A549 cells. Accordingly, the IC_{50} of CD-PEI-DOX in A549/ADM cells were markedly higher (151.7μg/mL) than that (6.72μg/mL) in the A549 cells. When CD-PEI-DOX were loaded with MRP1 siRNA sequences, the cells became more vulnerable to CD-PEI-DOX, IC_{50} was only 17.4μg/mL in A549/ADM cells. The CD-PEI has been proved to be non-toxic to cancer cells and normal cells, as shown in Fig. S3.

Based on these findings, we conclude that the free DOX exhibited different toxic behavior to A549 and A549/ADM cells. While CD-PEI-DOX-siMRP1 treatment caused more toxicity to A549/ADM cells compared with free DOX and CD-PEI-DOX groups at all-time points. It indicated that CD-PEI-DOX-siMRP1

possess better antitumor effect than DOX and CD-PEI-DOX. CD-PEI-DOX-siMRP1 possesses high toxic to A549/ADM due to the co-delivery and synergistic effect of siRNA and DOX, indicating that the MRP1 was critically involved in chemoresistance of A549/ADM cells against doxorubicin. The CD-PEI have the capability of transfection siRNA to the cells and interfere the expression of MRP1. Fig. 4D shows that the expression of MRP1 in A549/ADM cell could be suppressed by CD-PEI-DOX-siMRP1.

These results led us to postulate: whether MRP1 was induced by CD-PEI-DOX and suppressing MRP1 would reverse this effect? To test our hypothesis, we treated both A549 and A549/ADM cells with the indicated drugs and analyzed the expression of MRP1 after treatment. As demonstrated in Fig. 4F-4F, the expression of MRP1 increased markedly in case of CD-PEI-DOX treatment. In contrast, MRP1 expression decreased after siRNA targeting MRP1 only in A549/ADM cells (Fig. 4F) was loaded on CD-PEI-DOX particles. Combined with the cell viability results, knockdown the expression of MRP1 augment the killing effect of CD-PEI-DOX. **The internalization of DOX and nanodrug system based on CD-PEI**

The cellular uptake efficiency of free DOX, and CD-PEI-DOX-siMRP1 has been studied by laser scanning confocal microscopy and flow cytometry. The A549 and A549/ADM cells were incubated for 24 hours with PBS, free DOX, CD-PEI-DOX, CD-PEI-DOX-siNC, and CD-PEI-DOX-siMRP1, respectively. The results revealed that more CD-PEI-DOX-siMRP1 is uptaken by the cell and located in the perinuclear regions and the nuclei. The phenomenon revealed that the CD-PEI-DOX-siMRP1 could enhance the permeability of DOX in to the nuclei, which is beneficial to increase the therapeutic efficiency of DOX. In the A549/ADM, the CD-PEI-DOX-siMRP1 may increase the uptake efficiency of the DOX into the cell, and the DOX wrapped by nanocarrier could enter into the A549/ADM more than the free DOX group, for the reason that the nano carrier may increase the permeability of free drug into the cells. The permeability of free DOX, and DOX wrapped by CD-PEI has been investigated using A549 and A549/ADM cell spheres by the Z-stack mode of laser scanning confocal microscopy. The Z-stack mode could be used to observe the penetrate situation of different treatment by gaining the different layers of the cell mammosphere. The results revealed that the group treated by free DOX has the weakest permeability among all the groups. And the CD-PEI-DOX-siMRP1 could penetrate the inner region of mammosphere, as shown in Fig. 6. This result confirmed that the CD-PEI-DOX-siMRP1 could have the permeability to enter into the tumor tissue, which can maximize the therapeutic effect.

The uptake of DOX and nanodrug system has been measured by flow cytometry. Fig. 7 is the uptake in A549 and A549/ADM cells during the different intervals. The group incubated with CD-PEI-DOX-siMRP1 have higher mean fluorescence intensity than other group in both A549 and A549/ADM, indicated that CD-PEI-DOX-siMRP1 could delivery more DOX into cell. The cellular uptake of free DOX is lower than other treated groups at every interval in both A549 and A549/ADM cells. The nanodrug could decrease the drug efflux and gather high intracellular concentration of the drug, because the nanodrugs bypass the efflux pumps. And in the A549/ADM, the uptake amount of CD-PEI-DOX-siMRP1 is higher than other groups, results from the disrupting of siRNA to cellular pathway. This result indicated that the disturbing MRP1 could enhance the uptake of nanodrug effectively. The co-delivery DOX and siRNA would more effective in overcoming resistance of cancer cells.

CD-PEI and CD-PEI-siMRP1 enhanced the inhibitory effect on stemness and metastatic potential elicited by doxorubicin

The ability of metastasis is the critical factor that influence the therapeutic efficiency of tumor. We used the Transwell assay to investigate the migration and invasion in A549 and A549/ADM cells affected by respective drugs. Both A549 and A549/ADM treated with DOX, CD-PEI-DOX and CD-PEI-DOX-siNC and CD-PEI-DOX-siMRP1 exhibited decreased migration and invasion compared to the control, with migration counts shown in Fig. 8, respectively. The results indicated that CD-PEI-DOX and CD-PEI-DOX-siNC and CD-PEI-DOX-siMRP1 generated stronger inhibitory effects than free DOX. We found that CD-PEI-DOX distinctly inhibited the migration and invasion of both A549/ADM and ADM cells compared with the group treated by free DOX. After silencing MRP1, the decline in migration and invasion was reversed elicited by CD-PEI-DOX treatment in chemoresistant A549 cells. These results collectively showed that MRP1 is critical for mediating the chemoresistant effect of A549 against doxorubicin.

To elucidate the regulation of stemness in lung cancer by MRP1, we conducted sphere-forming assays. As revealed in Fig. 9, CD-PEI-DOX-siMRP1 treatment specifically suppressed the size and number of spheres in A549/ADM cells. A conclusion could be drawn from the above findings that suppressing MRP1 expression attenuated the resistance to regulation of stemness, migration and invasion induced by CD-PEI-DOX in DOX-resistant A549 cells.

Targeting and biocompatibility analysis of CD-PEI-DOX-siMRP1

Based on the *ex vivo* results, we conducted *in vivo* experiments to analyze the targeting of CD-PEI-DOX-siMRP1. As shown in Fig. 10A, specific binding of CD-PEI-DOX-siMRP1 particles were observed, while no marked binding were seen in free doxorubucin treated group. CD-PEI-DOX-siMRP1 located on tumors specfically at 12h. Tumors and organs were harvested, the fluorescence intensity were stastistically analyzed (n=3). CD-PEI-DOX-siMRP1 bear strong binding on tumors compared with dox group (Fig. 10B-10C). Hemolysis assays were conducted to analyze the toxic effect of our nanodrugs. The results revealed that CD-PEI-DOX-siMRP1 have no obvious toxic effect on blood among all groups, even at high concentration. Triton X-100 was included as a positive control (Fig. 10D-10E). Strong biocompatibility of CD-PEI-DOX-siMRP1 could be concluded since no obvious changes were seen in routine blood test (Fig. 10F). Suseuqently, slices from organs of each group were obtanied and subjected to HE staining. No destructive structures of drugs on different organs were seen (Fig. 10G). These results collectively show that CD-PEI-DOX-siMRP1 consistently target tumor and bear good biocompatibility and no obvious toxic effect *in vivo*.

Conclusion

In this work, we offered a new approach to overcome the chemoresistance through a strategy of combining siRNA targeted to the MRP1 with chemotherapeutic by the co-delivery system based on CD-PEI. The surface of carbon dots was decorated with PEI groups, having the capability of carrying siRNA, and the DOX agent was loaded through electrostatic interactions. The co-delivery systems effectively

loaded and released siRNA and DOX agents to the targeted tumor, overcoming the resistance to chemotherapy. By suppressing MRP1, CD-PEI-DOX-siMRP1 can obviously increase the drug intercellular accumulation and inhibit the cancer cell proliferation. The migration and invasion of A549/ADM cells were inhibited by CD-PEI-DOX-siMRP1. These results confirmed that the co-delivery systems enhance the therapy efficiency and overcome the chemoresistance. CD-PEI-DOX-siMRP1 co-delivery systems could inhibit the proliferation, migration, and invasion of the cancer cell because of the synergistic treatment from siRNA and anti-cancer agent. These works pave the way for exploring the application of co-delivery system underlying chemoresistance of anti-cancer drugs in treatment of lung cancer.

Materials And Methods

The synthesis of CD-PEI

CD-PEI was fabricated by the microwave-assisted method with PEI-passivated at the surface. The glycerol and PBS solution (pH 7.4) have been mixed togather, and PEI (MWCO, 25 kDa) was added into the homogeneous solution. The mixed solution has been transform into a beaker, and placed into a microwave oven (80P) for heating 10 minutes. Then, the reaction product was diluted by 10 mL ultrapure water and dialysised for 2 days to remove the unreacted agents. The solution after dialysis was lyophilized and stored at 4 ℃.

The characterization of CD-PEI and a nanodrug system based on CD-PEI

The TEM image of CD-PEI was obtained by high-resolution transmission electron microscopy (JEM-2100) and the X-ray photoelectron spectroscopy of CD-PEI and CD-PEI-DOX were measured by a Thermo 250Xi Thermo K-Alpha. The UV-Vis absorbance spectra of the CD-PEI, CD-PEI-DOX, CD-PEI-DOX-siNC, and CD-PEI-DOX-siMRP1 were measured by a Shimadzu UV3600. The PL spectra were characterized by a flourescence spectrofluorometer (Edinburgh, FLS 980-STM).

The loading and releasing of DOX

The DOX was loaded onto CD-PEI by electrostatic interactions, which has been studied in our previous work[10]. Brifely, the CD-PEI solution mixed with DOX was shaked for 24 h at 4 ℃ and then dialysised for 3 days to remove the excess DOX agent. The 40 nmol/L MRP1 siRNA was added into the CD-PEI-DOX solution and shaked for 24 h at 4 ℃ in order to combine them through electrostatic interactions.

The drug loading efficiency of DOX was calculated by the absobance at 480 nm. The DOX releasing by CD-PEI-DOX-siMRP1 was measured by the drug release experiment as following: 2 mL CD-PEI-DOX-siMRP1 solution was added into a dialysis bag (MWCO, 3 kDa), and soaked into PBS solution. After incubation for different interval, 1 mL PBS solution was gathered and fresh same volume PBS solution was added. The CD-PEI solution was placed under a 5 W UV flashlight with an excitation wavelength of 365 nm. The drug loading efficiency (DLE) was calculated as follows:

DLE% = (amount of DOX in CD-PEI-DOX/amount of DOX) ×100%.

Cell culture

The human lung cancer cells (A549) and doxorubicin-resistant lung cancer cells (A549/ADM) were cultured in Dulbecco's Modified Eagle's Medium (DMEM). The 10% fetal bovine serum (FBS), 1% penicillin(100 unit mL^{-1}) and streptomycin (100 μg mL^{-1}) (Gibco, Carlsbad, CA, USA) were added into the DMEM solution. The cells were cultured in a incubator with 5% CO_2 at 37 °C.

Cell cytotoxicity

The Cell Counting Kit-8 (CCK8) was used to measure the cell viability. 1×10^4 of A549 and A549/ADM cells were seeded in 96-well plates for 24 hours. The PBS, free DOX, CD-PEI-DOX, and CD-PEI-DOX-siMRP1 were added into the DMEM with different concetrations and incubated for 48 hours. Then, the cells were rinsed and added medium with CCK8 for 1 hours. The absorbance at 450 nm was measured by a spectrophotometer.

Intracellular drug release

A549 and A549/ADM cells were seeded and cultured on the Φ15 mm glass battern cell culture dish, respectively. The PBS, free DOX (20μg/mL), CD-PEI-DOX (DOX concetration, 20μg/mL), CD-PEI-DOX-siNC (DOX concetration, 20μg/mL), and CD-PEI-DOX-siMRP1 (DOX concetration, 20μg/mL) have been added into the culture dish and incubated for 24 hours. After incubation, the cells were rinsed by PBS and observed by confocal laser scanning microscopy (Zeiss LSM 880, Jena, Germany). A549 and A549/ADM cells manmospheres were seeded in the cofocal dish and incubated with nanodrug for 24 houres.

Cellular uptake *in vitro*

6×10^5 of A549 and A549/ADM cells have been seeded in the petri dish, respectively. And the cells were treated by different group, such as PBS, free DOX, CD-PEI-DOX, CD-PEI-DOX-siNC, and CD-PEI-DOX-siMRP1 for different inbucation time. And the cells were collected to measure the geometric mean fluorescence intensity by flow cytometry in Y610-mCHERRY channel (Beckman cytoflex LX).

The transwell assays

The migration and invasion assays of the A549/ADM and A549 evaluating metastasis ability were performed in 24-well transwell chambers with 8 μm size pores (Costar, Washington, D.C., USA). And the pores were covered with 100 μL of Matrigel (BD, USA) in the invasion assay. A549/ADM and A549 were added PBS, DOX, CD-PEI-DOX, CD-PEI-DOX-siNC and CD-PEI-DOX-siMRP1 and incubated for 24 hours. The DOX concetrations of A549/ADM and A549 are 60 μg/mL and 30 μg/mL, respectively. Then, 8×10^4 cells in 200 μL serum-free DMEM were seeded in the upper chambers and 700 μL of medium supplemented with 10% fetal bovine serum was added in the lower chamber. After 24h of incubation in 37 °C, 5% CO_2, the upper chambers were removed, and cells on the lower face of the membranes were fixed with 4% fixative solution (Solarbio, Beijing, China) and stained with Crystal violet. We counted the

number of migrated or invaded cells under 5 randomly selected fields at ×100 magnification by inverted light microscope (Leica DMi1, Wetzlar, Germany) for three times independently.

RNA isolation and qPCR analysis

Total Cell RNA isolation and cDNA synthesis were finished with the PrimeScript™ RT reagent Kit (TaKara Bio, USA) following the protocol. The concentration and integrity of RNA was determined using the 260/280 ratios generated by a Nano-drop UV spectrophotometer. Gene-specific primers were designed and synthesized by IGE BIOTECHNOLOGY (Guangzhou, China). qPCR was performed using PrimeScript RT Enzyme Mix I according to the manufacturer's instructions in CFX96™ Real-Time System (C1000 Thermal Cycler Class, Bio-Rad, California, USA). The two-step PCR conditions used are as follows: Pre-denaturation at 95 °C for 30 second; 40 cycles of (denaturation at 95 °C for 5 second, annealing and extension at 60 °C for 30 second), and denaturation for 10 second. And then melting curve stage was followed from 60 to 95 °C with increment 0.5 °C for 20 second while scanning for fluorescence. Relative quantitation was performed using the $2-\Delta\Delta Ct$ method and data were normalized against GAPDH. Primers sequences for MRP1 and GAPDH are as follows: MRP1: 5'-CCGTGTACTCCAACGCTGACAT-3' and 5'-ATGCTGTGCGTGACCAAGATCC-3'; GAPDH: 5'-TGTGGGCATCAATGGATTTGG-3' and 5'-ACACCATGTATTCCGGGTCAAT-3'.

In vitro transfection

A549/ADM cells (4×10^5) were seeded in 6-well plates and incubated for 24h. The solutions of siMRP1-lipid complex complexes (50 nmol/L siMRP1) or CD-PEI-siMRP1 complexes were prepared before transfection. The medium was replaced by 1mL Opti-MEM per well and the two kind of siMRP1 mixture were separately added to each well. After 12 h transfection, the culture medium was replaced with the fresh complete medium and cells were incubated for an additional 36 h for flow cytometry (FCM). The siRNA are purchased from RiboBio Co., Ltd.(Guangzhou, China) and the number of NC is siN0000001-1-5 siR. The sequences for siMRP1 are as follows: stB0001371B genOFFTM st-h-MRP1_001: GACCTCCGCTTCAAGATCA; stB0001371B genOFFTM st-h-MRP1_002: CCGTCTACGTGACCATTGA; stB0001371B genOFFTM st-h-MRP1_003: CTGGGCTTATTTCGGATCA.

Western blot assays

Western blot assays were carried out as previously described[26]. Breiefly, total cell lysates were prepared in RIPA buffer (Beyotime, Shanghai, China). and proteins were separated by the sodium dodecyl sulfate-polyacrylamide gel electrophoresis (SDS-PAGE) and transferred to nitrocellulose membranes. After blocking with 5% skim milk for 2 h, the membranes were incubated with the primary antibodies against MRP1 (Cell Signaling Technology, Boston, MA, USA), ABCG2 (Cell Signaling Technology, Boston, MA, USA), P-gp (GeneTex, Irvine, CA, USA), and then incubated with the secondary HRP-conjugated antibody (1:5000, Zhongshan Goldenbridge, Beijing, China). Protein bands were visualized using ECL detection reagent and normalized by β-actin (Cell Signaling Technology, Cell Signaling Technology, Boston, MA, USA). Triplicate individual experiments were performed in this study.

Growth inhibition of sphere forming.

A549 and A549/ADM cells were treated by free DOX, CD-PEI-DOX, CD-PEI-DOX-siNC, CD-PEI-DOX-siMRP1 for 24h, respectively. The cells were digested and seeded onto 6-well plates and cultured in DMEM/F12 medium (GIBCO) contained with 4 μg/mL insulin B27 (1:50), 20 ng/mL EGF and 10 ng/mL FGF. The morphology and diameters of spheres were measured after an additional 5 days.

Animal Study *in vivo*

All animal studies were approved by Animal ethics committee of the Fifth Affiliated Hospital Sun Yat-sen University. Briefly, A549 cells were subcutaneously inoculated into 4 weeks old male Balb/c nude mice to construct xenograft models. When tumors grew to palpable size, DOX and CD-PEI-DOX-siMRP1 were injected through tail vein. The bio-distribution of drugs were visualized by in vivo image system (IVIS) equipment. Hemolysis experiment were performed to assess the biocompatibility of drugs. The targeting of drugs on tumor were viusualized and photographed as the indicated time points. Penetration of the drugs into tumor were obtained using confocal microscopy LSM880 (Zeiss).

Immunohistochemical assays

Tumor and organs were obtained after mouse were scarificed humanely. Slices were prepared from frozen tissues. Immunohistochemical staining were conducted as prveiously described. Hematoxylin and eosin (H&E) staining (ZSBG-BIO, Beijing, China) were carried out to investigate the toxic effect of drugs. Representative pictures were shown and the distribution of different drugs were visulized undrer optical microscopes (BX53 System Microscope, Olympus, Japan).

Statistical analysis

The data between groups was statistical analyzed by Student’s t-test. $P<0.05$ was used as the criterion for statistical significance.

Abbreviations

CD:

carbon dots

PEI:

poly-ethylenimine

Dox:

doxorubicin

siRNA:

small interfer RNA

ATP:

Adenosine triphosphate

IC50 :

half maximal inhibitory concentration

MRP1:

multidrug resistance-associated protein 1

A549

human non-small cell lung carcinoma cell line

A549/ADM:

multidrug resistant human non-small cell lung carcinoma cell line

QDs:

quantum dots

PL:

photoluminescence

CCK8:

the Cell Counting Kit-8

SDS-PAGE:

sodium dodecyl sulfate-polyacrylamide gel electrophoresis

PVDF:

polyvinylidene difluoride

IVIS:

in vivo image system

DLS:

dynamic light scattering

ABCG2:

ATP-binding cassette transporter, sub-family G, member 2

P-gp:

P-glycoprotein

Declarations

Ethics approval and consent to participate

The study received approval from the institutional review board of the Fifth Affiliated Hospital Sun Yat-sen University.

Consent for publication

Not applicable.

Declaration of interest

The authors declare that they have no known competing financial interests or personal relationships that could have appeared to influence the work reported in this paper.

Availability of data and materials

Data sharing is not applicable to this article as no datasets were generated or analyzed during the current study.

Funding:

The Fundamental Research Funds for the Central Universities (19ykpy42)

The Guangdong Basic and Applied Basic Research Foundation (2020A1515011001)

Author contributions:

Yu Hailing performed the experiments including synthesis and characterization of the nanodrug and wrote the whole paper. Luo Hui carried out the in vivo experiments with Lin Xi. Huang Kaicheng conducted in vitro experiments together with Tang Kexin. All the co-first author analyzed all the data in the article. Yang Lei, and Wu Lili helped to conduct the synthesis and characterization of the drug. Mei Chaoming helped to perform in vitro experiments.

Acknowledgments

We owe gratitude to Huang Yongquan for his support in hemolysis and routine blood test experiments. We also appreciate guidance from Zhang Qianqian in trans-well experiments. This work was supported by the Fundamental Research Funds for the Central Universities (19ykpy42), the Guangdong Basic and Applied Basic Research Foundation (2020A1515011001).

Declarations

Affiliations

Guangdong Provincial Key Laboratory of Biomedical Imaging and Guangdong Provincial Engineering Research Center of Molecular Imaging, The Fifth Affiliated Hospital, Sun Yat-Sen University, Zhuhai, P. R. China

Luo Hui, Tang Kexin, Lin Xi, Mei Chaoming, Yu Hailing

Institute of Antibody Engineering, School of Laboratory Medicine and Biotechnology, Southern Medical University, Guangzhou, P. R. China

Huang Kaichen

Key Laboratory for Photonic and Electronic Bandgap Materials, Ministry of Education, School of Physics and Electronic Engineering, Harbin Normal University, Harbin, P. R. China

Center for Engineering Training and Basic Experimentation, Heilongjiang University of Science and Technology, Harbin, P. R. China

Wu Lili

Center for Composite Materials and Structures, Harbin Institute of Technology, Harbin, P. R. China

Yang Lei

References

1. F. Bray, A. Jemal, N. Grey, J. Ferlay and D. Forman, "Global cancer transitions according to the Human Development Index (2008-2030): a population-based study," *Lancet Oncol* vol. 13, no. 8, pp. 790-801, 2012.
2. R. J. Kathawala, P. Gupta, C. R. Ashby and Z.-S. Chen, "The modulation of ABC transporter-mediated multidrug resistance in cancer: A review of the past decade," *Drug Resistance Updates*, vol. 18, pp. 1-17, 2015.
3. M. Bar-Zeev, Y. D. Livney and Y. G. Assaraf, "Targeted nanomedicine for cancer therapeutics: Towards precision medicine overcoming drug resistance," *Drug Resistance Updates*, pp. 15-30, 2017.

4. M. M. Gottesman, "Mechanisms of Cancer Drug Resistance," *Annual Review of Medicine*, vol. 53, no. 1, pp. 615-627, 2002.
5. O. Taratula, "Innovative Strategy for Treatment of Lung Cancer: Inhalatory Codelivery of Anticancer Drugs and siRNA for Suppression of Cellular Resistance," *Journal of Drug Targeting*, vol. 19, no. 10, pp. 900-914, 2011.
6. M. Creixell and N. A. Peppas, "Co-delivery of siRNA and therapeutic agents using nanocarriers to overcome cancer resistance," *Nano Today*, vol. 7, no. 4, pp. 367-379, 2012.
7. N. Licciardello, S. Hunoldt, R. Bermann, G. Singh, C. Mamat, A. Faramus, J. L. Z. Ddungu, S. Silvestrini, M. Maggini and L. De Cola, "Biodistribution studies of ultrasmall silicon nanoparticles and carbon dots in experimental rats and tumor mice," *Nanoscale*, pp. 10.1039.C1038NR01063C, 2018.
8. S. Hettiarac, R. Graham, K. J. Mintz, Y. Zhou, S. Vanni, Z. Peng and R. Leblanc, "Triple conjugated carbon dots as a nano-drug delivery model for glioblastoma brain tumors," *Nanoscale*, 2019.
9. N. Gao, W. Yang, H. Nie, Y. Gong, J. Jing, L. Gao and X. Zhang, "Turn-on theranostic fluorescent nanoprobe by electrostatic self-assembly of carbon dots with doxorubicin for targeted cancer cell imaging, in vivo hyaluronidase analysis, and targeted drug delivery," *Biosens Bioelectron*, vol. 96, pp. 300-307, 2017.
10. H. Yu, X. Lv, L. Wu, B. Li and H. Shan, "Doxorubicin-loaded fluorescent carbon dots with PEI passivation as a drug delivery system for cancer therapy," *Nanoscale*, vol. 12, no. 33, pp. 17135-17558, 2020.
11. H. Ding, F. Y. Du, P. C. Liu, Z. J. Chen and J. C. Shen, "DNA-Carbon Dots Function as Fluorescent Vehicles for Drug Delivery," *Acs Applied Materials & Interfaces*, vol. 7, no. 12, pp. 6889-6897, 2015.
12. S. Karthik, B. Saha, S. K. Ghosh and N. D. P. Singh, "Photoresponsive quinoline tethered fluorescent carbon dots for regulated anticancer drug delivery," *Chemical Communications*, vol. 49, no. 89, pp. 10471-10473, 2013.
13. D. C. Ihde, "Chemotherapy of lung cancer," *N Engl J Med*, vol. 327, no. 20, pp. 1434-1441, 1992.
14. J. F. Lu, D. Pokharel and M. Bebawy, "MRP1 and its role in anticancer drug resistance," *Drug Metab Rev*, vol. 47, no. 4, pp. 406-419, 2015.
15. R. W. Robey, K. M. Pluchino, M. D. Hall, A. T. Fojo, S. E. Bates and M. M. Gottesman, "Revisiting the role of ABC transporters in multidrug-resistant cancer," *Nat Rev Cancer*, vol. 18, no. 7, pp. 452-464, 2018.
16. T. Du, J. G. Liang, N. Dong, L. Liu, L. R. Fang, S. B. Xiao and H. Y. Han, "Carbon dots as inhibitors of virus by activation of type I interferon response," *Carbon*, vol. 110, pp. 278-285, 2016.
17. Y. P. Sun, B. Zhou, Y. Lin, W. Wang, K. A. S. Fernando, P. Pathak, M. J. Meziani, B. A. Harruff, X. Wang, H. F. Wang, P. J. G. Luo, H. Yang, M. E. Kose, B. L. Chen, L. M. Veca and S. Y. Xie, "Quantum-sized carbon dots for bright and colorful photoluminescence," *Journal of the American Chemical Society*, vol. 128, no. 24, pp. 7756-7757, 2006.
18. S. N. Baker and G. A. Baker, "Luminescent Carbon Nanodots: Emergent Nanolights," *Angewandte Chemie-International Edition*, vol. 49, no. 38, pp. 6726-6744, 2010.

19. L. Yang, Z. R. Wang, J. Wang, W. H. Jiang, X. W. Jiang, Z. S. Bai, Y. P. He, J. Q. Jiang, D. K. Wang and L. Yang, "Doxorubicin conjugated functionalizable carbon dots for nucleus targeted delivery and enhanced therapeutic efficacy," *Nanoscale*, vol. 8, no. 12, pp. 6801-6809, 2016.
20. J. Hou, J. Yan, Q. Zhao, Y. Li, H. Ding and L. Ding, "A novel one-pot route for large-scale preparation of highly photoluminescent carbon quantum dots powders," *Nanoscale*, vol. 5, no. 20, pp. 9558-9561, 2013.
21. S. W. Zhang, J. X. Li, M. Y. Zeng, J. Z. Xu, X. K. Wang and W. P. Hu, "Polymer nanodots of graphitic carbon nitride as effective fluorescent probes for the detection of Fe3+ and Cu2+ ions," *Nanoscale*, vol. 6, no. 8, pp. 4157-4162, 2014.
22. M. Algarra, B. B. Campos, K. Radotic, D. Mutavdzic, T. Bandosz, J. Jimenez-Jimenez, E. Rodriguez-Castellon and J. C. G. E. da Silva, "Luminescent carbon nanoparticles: effects of chemical functionalization, and evaluation of Ag+ sensing properties," *Journal of Materials Chemistry A*, vol. 2, no. 22, pp. 8342-8351, 2014.
23. T. N. J. I. Edison, R. Atchudan, M. G. Sethuraman, J. J. Shim and Y. R. Lee, "Microwave assisted green synthesis of fluorescent N-doped carbon dots: Cytotoxicity and bio-imaging applications," *Journal of Photochemistry and Photobiology B-Biology*, vol. 161, pp. 154-161, 2016.
24. P. Yu, X. M. Wen, Y. R. Toh and J. Tang, "Temperature-Dependent Fluorescence in Carbon Dots," *Journal of Physical Chemistry C*, vol. 116, no. 48, pp. 25552-25557, 2012.
25. Y. Yuan, B. Guo, L. Hao, N. Liu, Y. Lin, W. Guo, X. Li and B. Gu, "Doxorubicin-loaded environmentally friendly carbon dots as a novel drug delivery system for nucleus targeted cancer therapy," *Colloids & Surfaces B Biointerfaces*, pp. 349, 2017.
26. X. Lv, H. Yu, Q. Zhang, Q. Huang, X. Hong, T. Yu, H. Lan, C. Mei, W. Zhang and H. Luo, "SRXN1 stimulates hepatocellular carcinoma tumorigenesis and metastasis through modulating ROS/p65/BTG2 signalling," *Journal of Cellular and Molecular Medicine*, vol. 24, pp. 10714-10729, 2020.

Tables

Table 1 IC_{50} of Free DOX, CD-PEI-DOX, CD-PEI-DOX-siMRP1 in A549 and A549/ADM cells

	IC_{50}(μg/mL)	
A549	Free DOX	26.993
	CD-PEI-DOX	6.72
	CD-PEI-DOX-siMRP1	5.692
A549/ADM	Free DOX	130.626
	CD-PEI-DOX	151.7
	CD-PEI-DOX-siMRP1	17.4

Figures

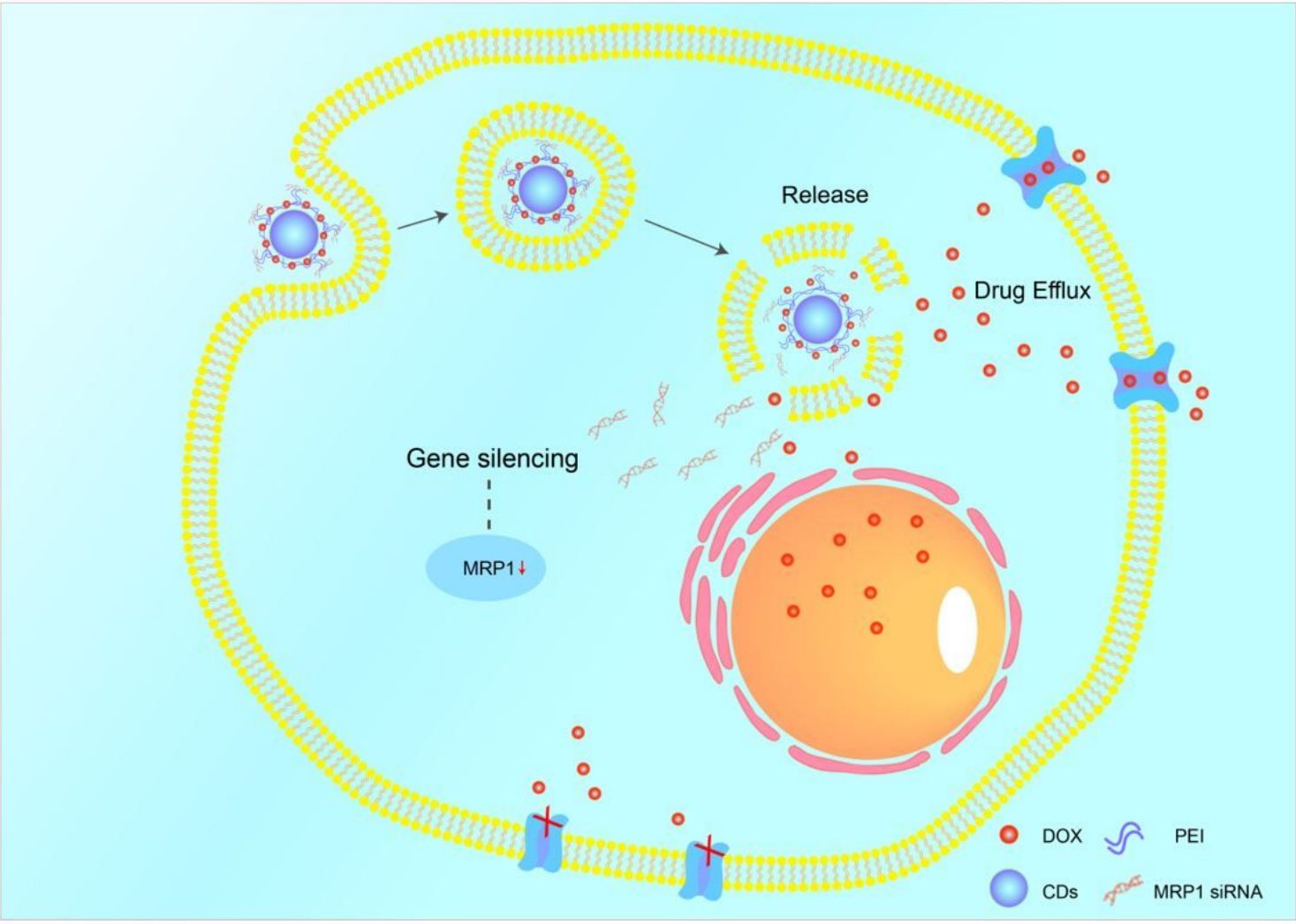

Figure 1

The schematic diagram of CD-PEI-DOX-siMRP1 overcomes the chemoresistance.

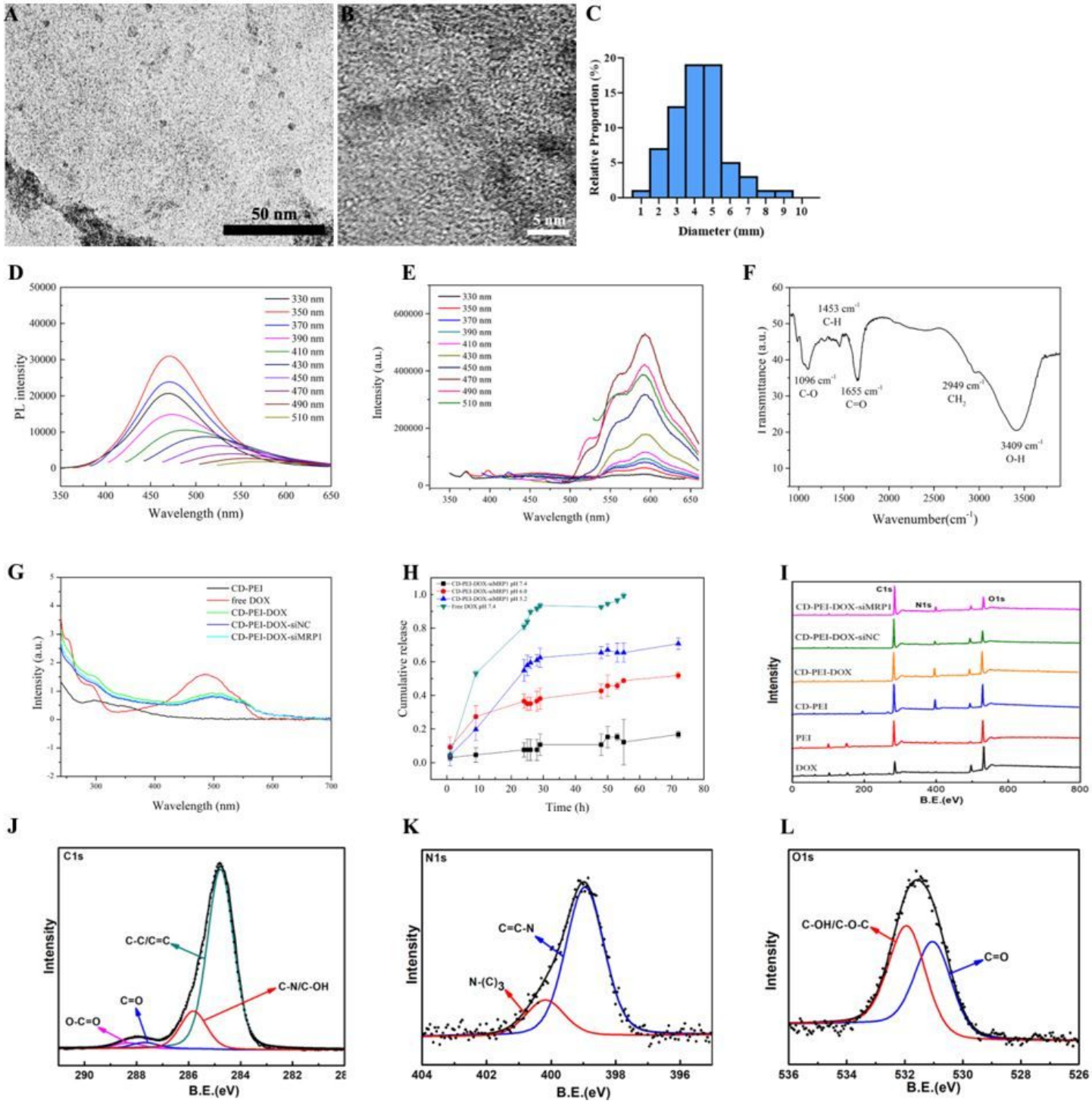

Figure 2

The characteristics of CD-PEI and CD-PEI-DOX-siMRP1. (A) and (B) The TEM images of CD-PEI. (C) The diameters distribution of CD-PEI. (D) The PL spectrum of CD-PEI-DOX-siMRP1. (E) The PL spectrum of CD-PEI and CD-PEI-DOX-siMRP1 under 470 nm exciation. (F) The UV-vis spectrum of CD-PEI, CD-PEI-DOX, CD-PEI-DOX-siNC, and CD-PEI-DOX-siMRP1. (G) The release behavior of CD-PEI-DOX-siMRP1 and free DOX under different pH. (I) XPS spectrum of PEI, DOX, CD-PEI, CD-PEI-DOX, CD-PEI-DOX-siNC, and CD-PEI-DOX-siMRP1. (J) C1s, (K) N1s and (L) O1s spectra of CD-PEI-DOX-siMRP1.

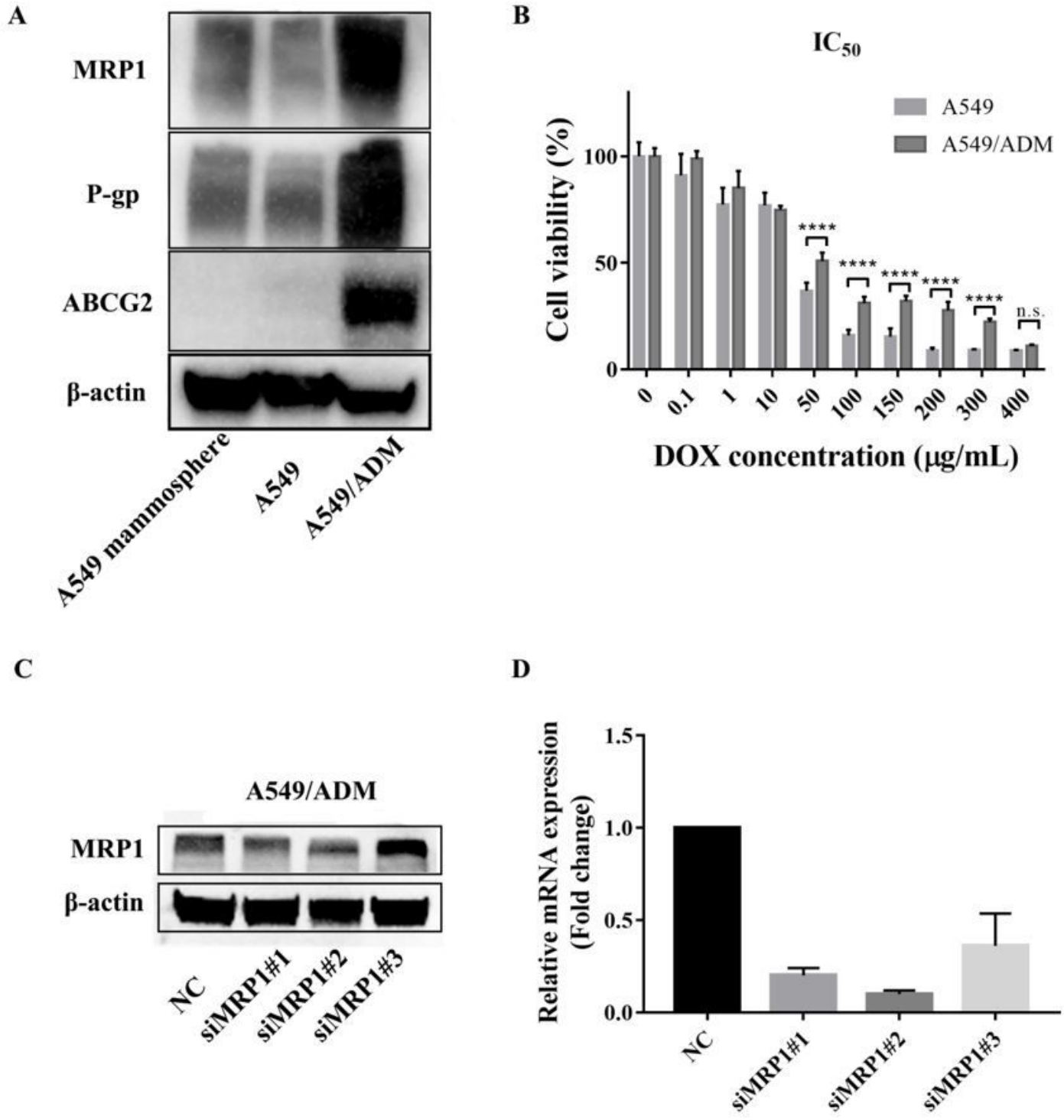

Figure 3

Analysis of chemoresistance of cells against doxorubicin. (A) Expression of MRP1, P-gp and ABCG2 on A549 and chemoresistant A549/ADM cells by western blot. β-actin was used as a loading control. (B) Cell viability was detected after treatment by indicated concentrations in A549 and A549/ADM cells. **** indicates $p<0.0001$. (C) The expression of MRP1 was detected by western blot after knockdown by three

siRNA sequences. (D) The expression of MRP1 was detected by qPCR after knockdown by three siRNA sequences.

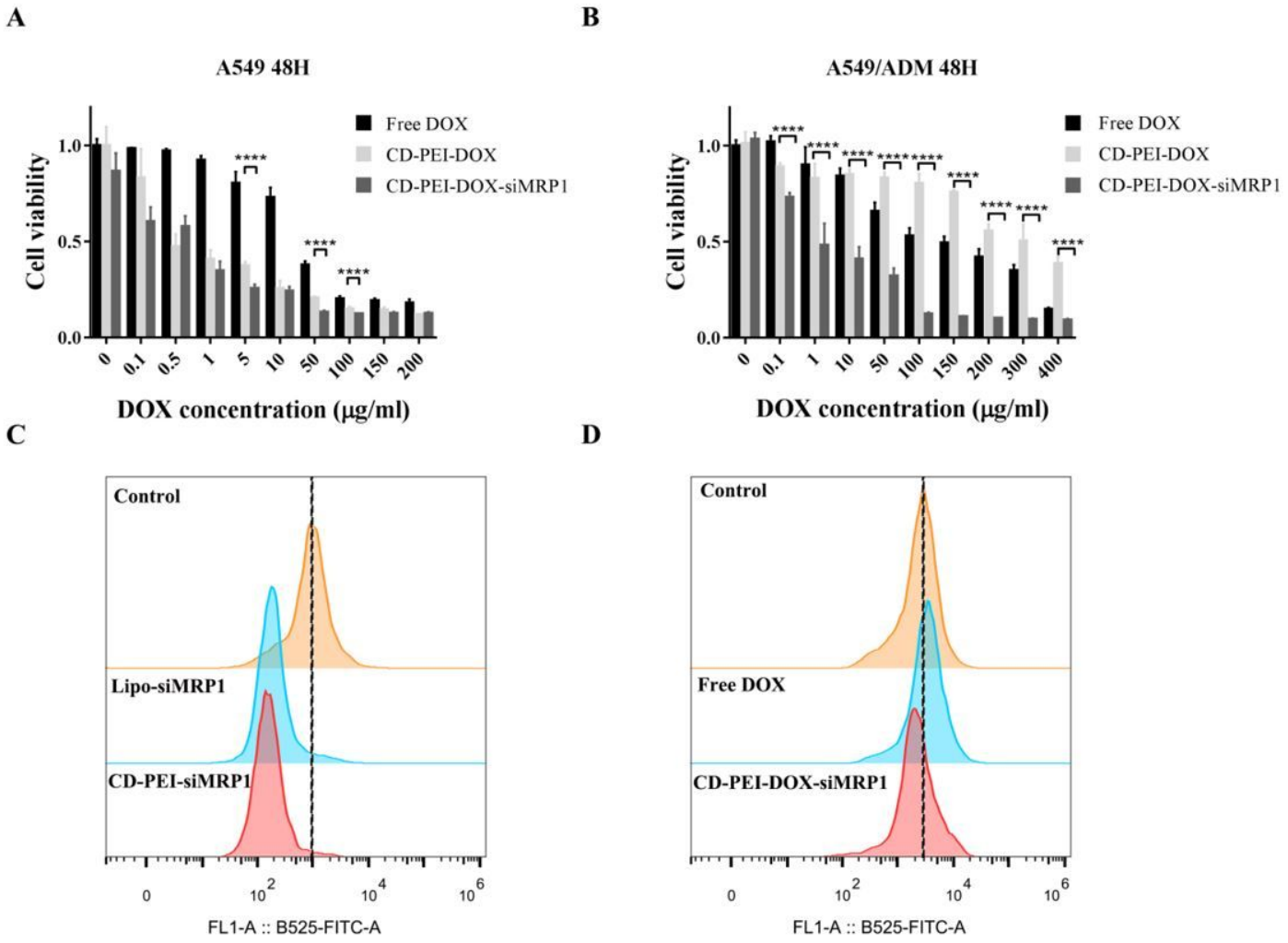

Figure 4

(A) and (B) The cell viability of A549 and A549/ADM cells incubation with free DOX, CD-PEI-DOX, and CD-PEI-DOX-siMRP1. (C) and (D) Expression of MRP1 on A549/ADM cells by flow cytometry.

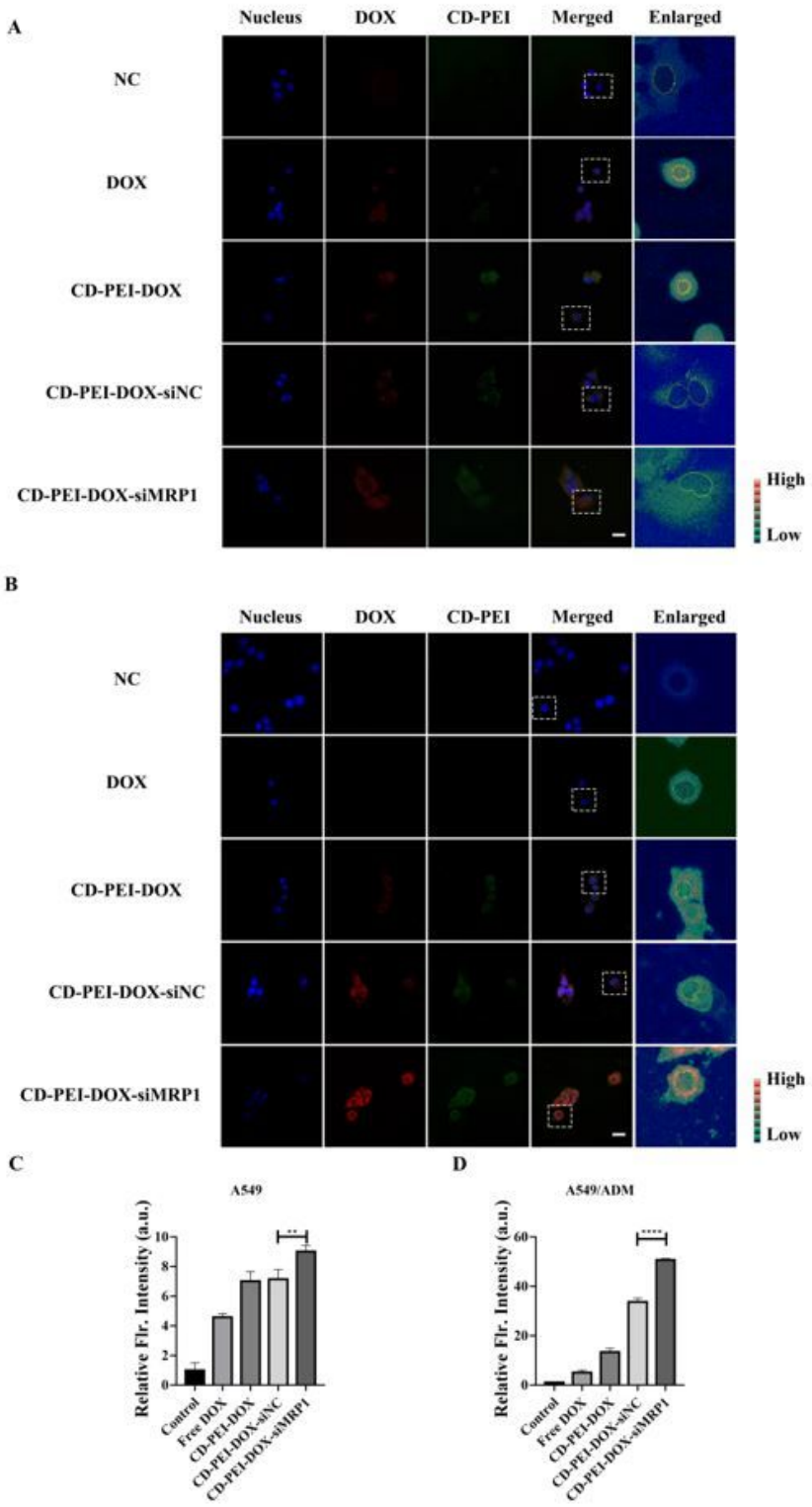

Figure 5

Immunofluorescence analysis of cells treated with indicated drugs. A549 (A) and A549/ADM (B) cells were treated with PBS, DOX, CD-PEI-DOX, CD-PEI-DOX-siNC, and CD-PEI-DOX-siMRP1 respectively. Representative pictures were taken under confocal microscopes using 40X oil lens. Blue and red signals indicate nucleus and doxorubicin. CD-PEI was manifested by green signals. Signals were merged using the same field. DOX distribution was reflected by densometric scale as shown in the fifth panel

(Enlarged). (C) and (D) The quantitative analysis of the fluorescence intensity of DOX by ImageJ. The scale bar is 20μm.

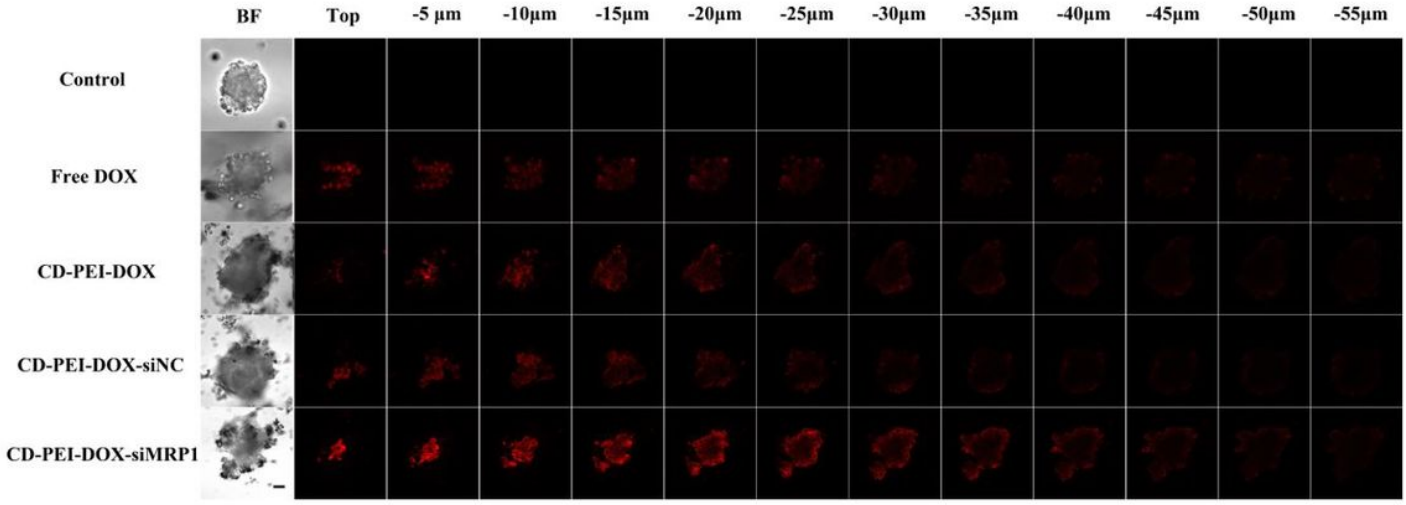

Figure 6

The penetration of drugs was detected using A549/ADM cells. Confocal Z-stack images of cell mammospheres were obtained and shown after incubation with PBS, free DOX, CD-PEI-DOX, CD-PEI-DOX-siNC, and CD-PEI-DOX-siMRP1. The bar is 20 μm.

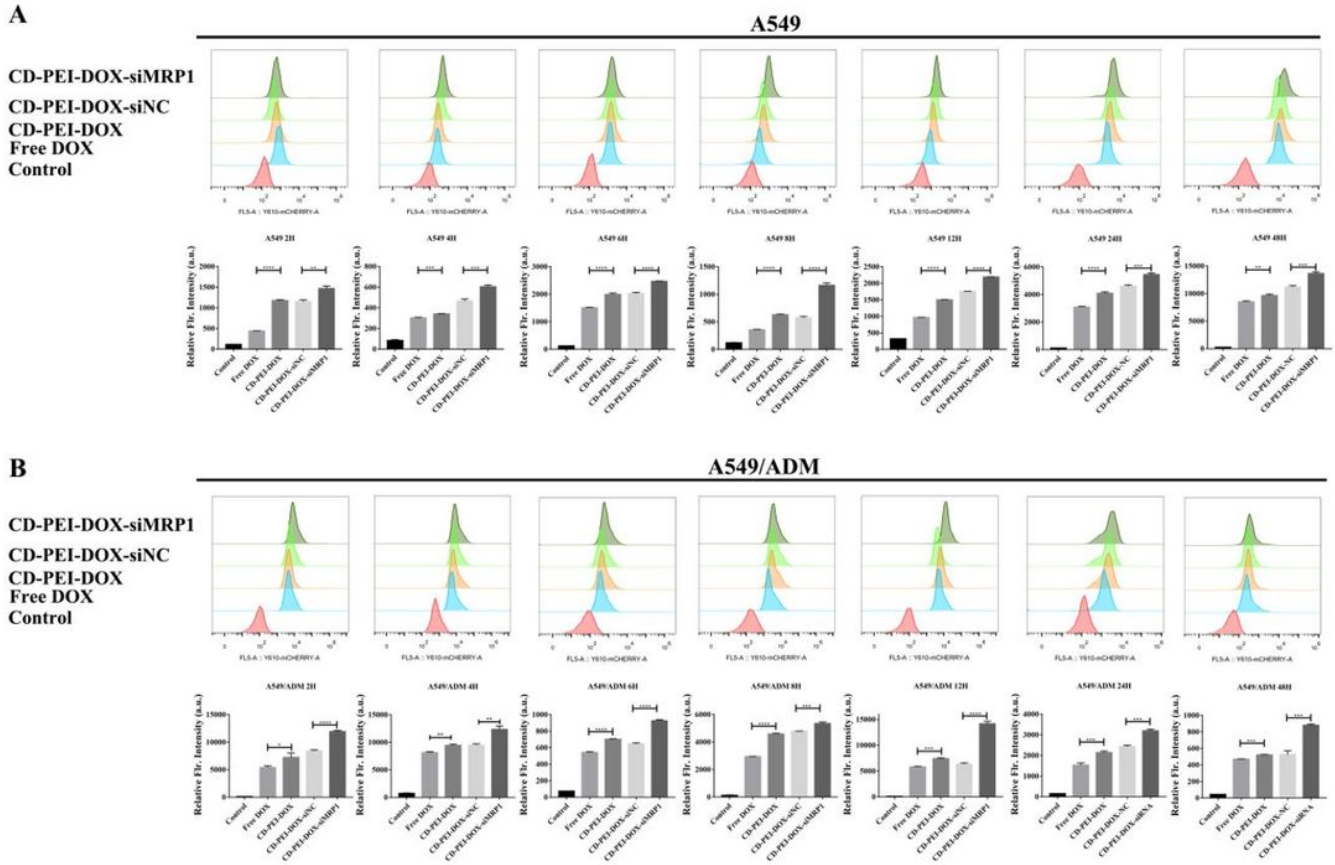

Figure 7

Uptake of drugs in A549/ADM and A549 cells were determined using flow cytometry. (A) Upper panel: A549 cells were treated with the drugs for the indicated periods, cells were collected and fluorescence signal of DOX were detected. Lower panel: Mean fluorescence intensity of each cell were calculated and statistically analyzed. (B) Upper panel: A549/ADM cells were treated with the drugs for the indicated time points, followed by FACs (fluorescence-activated cell sorting) analysis detecting the fluorescence of DOX. Lower panel: Statistically analysis of mean fluorescence intensity of DOX in each group. **** indicates p<0.0001.

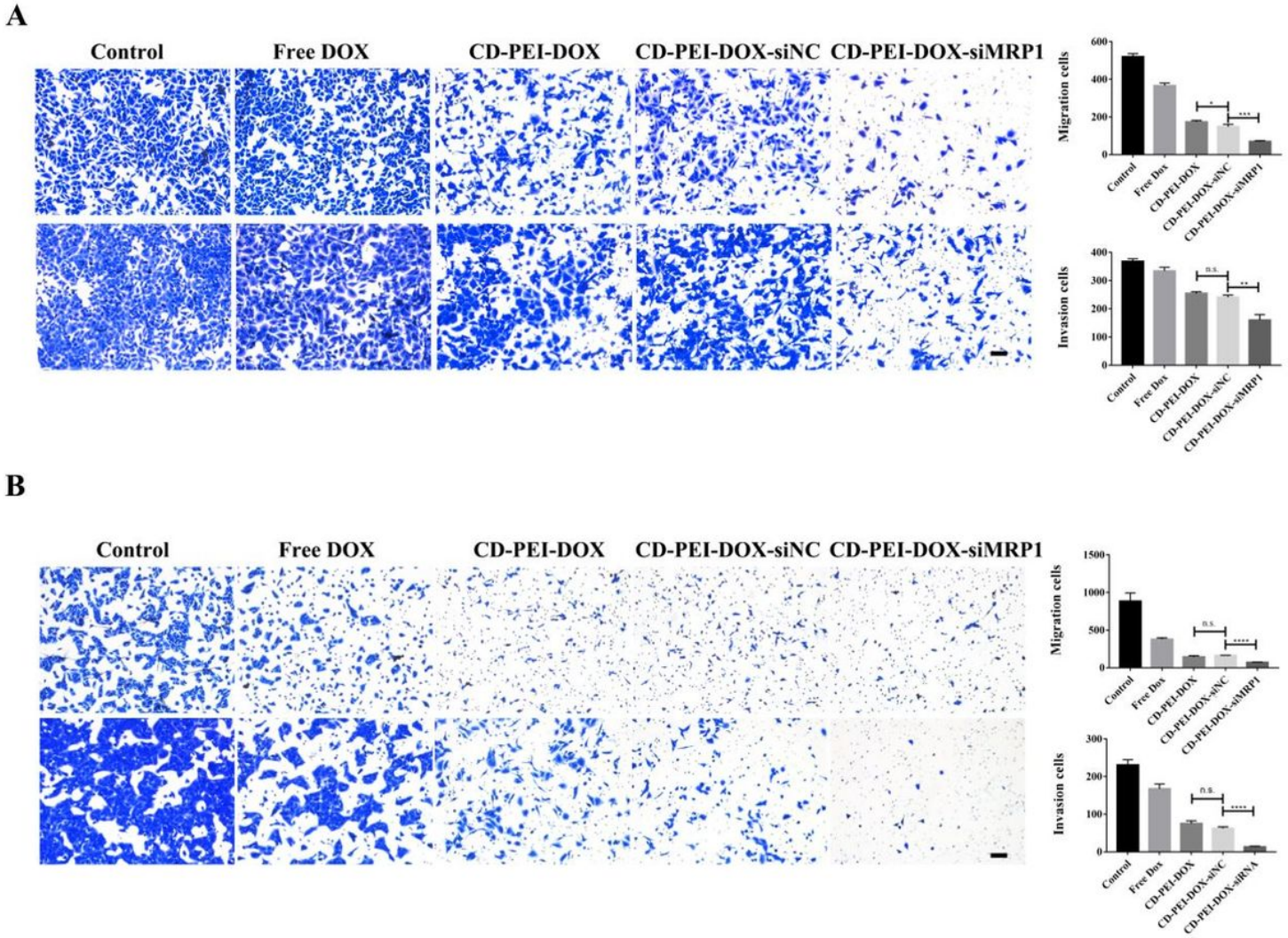

Figure 8

The transwell assay was performed to determine whether CD-PEI or CD-PEI-DOX-siMRP1 enhanced the inhibition effect of DOX. Microscopy images of the migration (Upper) and invasion (Lower) of A549 (A) and A549/ADM (B) cells that passed through the membrane after incubating with PBS, DOX, CD-PEI-DOX, CD-PEI-DOX-siNC and CD-PEI-DOX-siMRP1 compared with the control group (untreated cells). * p < 0.05. ** p < 0.01. *** p < 0.001. The scar bar is 200 μm.

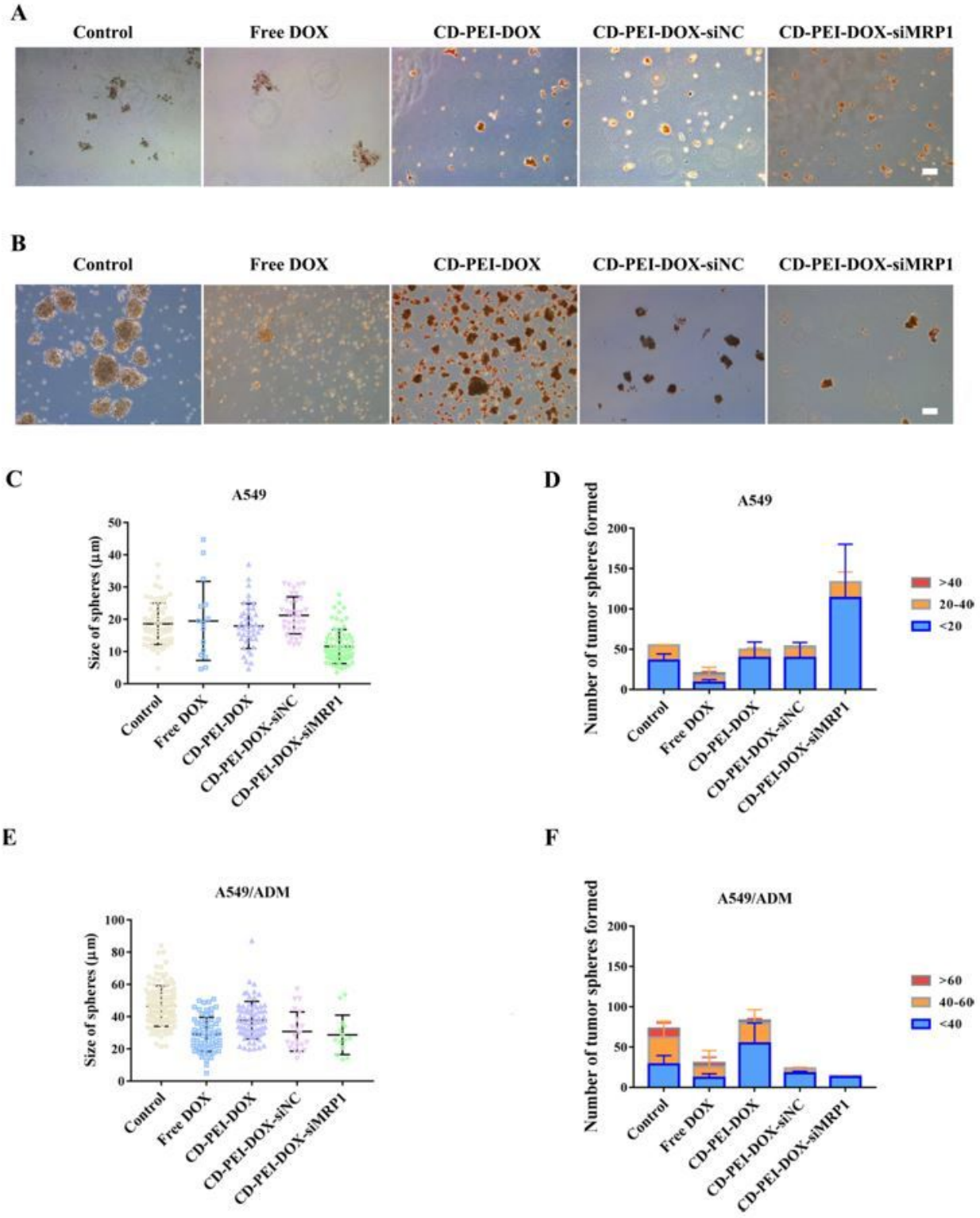

Figure 9

(A) and (B) The sphere forming assays of A549 and A549/ADM cells treated by PBS, DOX, CD-PEI-DOX, CD-PEI-DOX-siNC, and CD-PEI-DOX-siMRP1. (C) and (D) Relative sizes and numbers of sphere shown in A549 cells(A). (E) and (F) Relative sizes and numbers of sphere shown in A549/ADM (B).

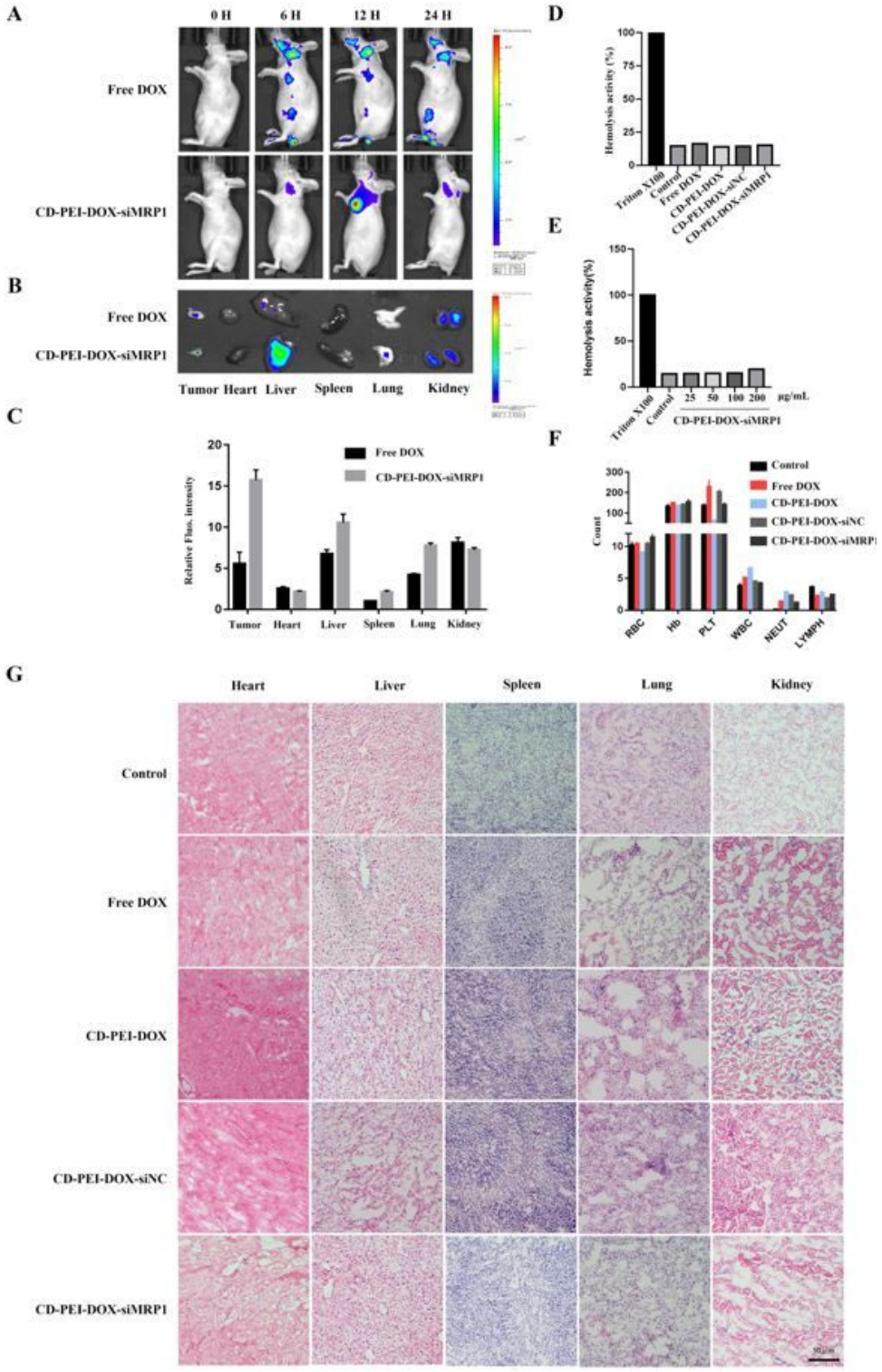

Figure 10

Analysis of targeting and biocompatibility of nanodrugs. (A) Free DOX and CD-PEI-DOX-siMRP1 were injected through tail vein in subcutaneous xenograft model. Pictures of representative time point were taken by IVIS. (B) Tumor and organs of representative group were harvested and photographed under IVIS. (C) Relative fluorescence intensity of each organ were calculated and statistically analyzed. (D) and (E) Hemolysis assays were conducted to analyze the toxic effect of different drugs as indicated and

dose-dependent toxic effect of CD-PEI-DOX-siMRP1 in on blood from volunteer. (F) Blood cells analysis was applied to analyze the biocompatibility of indicated drugs. (G) HE staining was conducted to determine the toxic effect of various drugs in indicated viscera .

Supplementary Files

This is a list of supplementary files associated with this preprint. Click to download.

- s1.jpg
- s2.jpg
- s3.jpg
- s4.jpg
- s5.jpg
- s6.jpg
- Graphicalabstract.docx
- Supplementrytable1.docx